International Journal of Scientific Engineering and Applied Science (IJSEAS) – Volume-3, Issue-4,April 2017
ISSN: 2395-3470
www.ijseas.com

Development of a biological tissue-like phantom for microwave imaging systems

Lulu Wang[1,*], Jingze Niu[1,2]
[1] School of Instrument Science and Opto-electronics Engineering, Hefei University of Technology, Hefei, China,

[2] Anhui Provence Hospital, Hefei, China
Correspondence: Lulu Wang, luluwang2015@hfut.edu.cn;

Abstract
Microwave imaging (MI) offers a promising complementary modality for breast imaging. With growing interest in MI modality for cancer detection, it is necessary to develop an artificial tissue-like phantom to simulate the interactions of electromagnetic waves within biological tissues. This paper presents the development of a biological tissue-like phantom using simple and cost-effective nature materials for investigation of MI techniques. Dielectric properties (DPs) of three fruits (cucumber, grape and blueberry) and two types of emulsifying ointment (EO) (EO-I: 30% emulsifying wax, 50% white soft paraffin and 20% liquid paraffin; EO-II: 27% emulsifying wax, 45% white soft paraffin and 18% liquid paraffin and 10% water) were measured at 10-20GHz and storage time 1~7 days. DPs of materials were measured by using an Agilent 85070 single port dielectric probe kit and an Agilent N5230A network analyzer. Based on the measured DPs of samples, two types of simplified tissue-like phantoms that contain skin (glass ceramic), healthy tissue (EO-II) and lesions (blueberry, grape) were developed and tested on a holographic microwave imaging system. DPs of grape, blueberry and two types of EO generally did not vary with frequency; the dielectric contrast between grape and EO-II, and that of blueberry and EO-II close to the contrast between real malignant and normal tissues. Microwave imaging results indicated that it is possible to produce a simplified biological tissue-like phantom using widely available low cost materials.

Keywords: *dielectric properties, microwave imaging, electromagnetic waves, biological tissues.*

1. Introduction

Microwave imaging (MI) has been intensely studied for breast cancer detection over the past few decades [1-5]. MI offers a promising complementary modality for breast imaging, which has potential for low-cost and pain-free breast imaging without harmful ionizing radiation [6]. With growing interest in MI modality for medical applications, it is necessary and important to develop an artificial tissue-like phantom for further investigation the interactions of electromagnetic waves in biological tissues. Dielectric properties (DPs) of biological tissues have been studied by many research groups [7-12]. Lazebnik et al. found that the DPs of breast tissue are primarily determined by the adipose content of each tissue sample [12]. The contrast between cancer tissue and normal tissue is 10:1. For example, the dielectric constant of cancer tissue is about 43 while the dielectric constant of normal tissue is about 4.3 at 10GHz. These research findings have been served as benchmarks in the design of breast phantoms.

Lagendijk and Nilsson used dough (consisting of flour, oil and saline) to model low-water-content tissues at 451 MHz [13]. Marchal et al. described a water–gelatin recipe to simulate high-water content tissues from 10 to 50 MHz [14]. Robinson et al. created materials to simulate muscle (ethanediol, water, salt and gelatin) and fat (ethanediol, gelatin and polyethylene powder) at 1000MHz [15]. Several materials have been used to simulate biological tissue-like phantoms [16-18]. Among these materials, gelatin-based materials are more attractive due to their stable mechanical properties and ease of fabrication. Oil-in-gelatin mixtures are commonly used to develop a breast phantom; however such phantom is hard to shape and does not include the heterogeneity of the breast. Polyacrylamide is not easy for fabrication due to the short life in air.

It is challenge to find suitable materials that can mimic different tissue properties over a wide range of frequencies and show similar dispersive behavior. This paper presents the development of biological tissue-like phantom using cost-effective nature materials. Various phantoms were developed and tested on a holographic microwave imaging (HMI) system. Various experiments were conducted to evaluate the effectiveness and performance of HMI using the developed phantom.

2. Methods

2.1. Holographic microwave imaging system and imaging processing

Figure 1 shows a HMI system that consists of a vector network analyzer (VNA), a testing table, an array of 16 antennas, and a computer with MATLAB GUI tool to produce microwave images. The 16-element antenna array is located under bottom of the table and surrounded with electromagnetic absorbing material to reduce ambient reflections. The optimization of antenna array

configuration was detailed in [19]. During operation, VNA excites microwave signals into the target object through the single transmitting antenna. The scattered electric fields from the target object are measured by receivers, which is connected to anther port of VNA via a multi-position switch. A computer with a matched computer programme is used to analyze the measured data by applying the imaging technique.

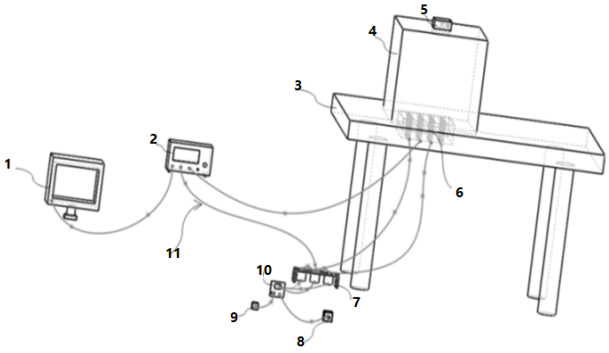

Figure 1. HMI measurement system, 1: computer with MATLAB GUI imaging tool; 2: VNA; 3：table; 4: polystyrene box bridge; 5: object; 6: an array of 16 antennas; 7-10: 16 channel switcher; 11: transiting cable.

Figure 2 shows a point P is within the interior of the target object. Under far-field, the complex visibility data for any pair of receivers is expressed [20]:

$$\overrightarrow{V_{i,j}} = < \vec{E}_{scat}(\vec{r_i}) \cdot \vec{E}^{*}_{scat}(\vec{r_j}) > \tag{1}$$

Where <> denotes the time average, $\vec{E}_{scat}$ is the scattered electromagnetic field from the object, $\vec{E}^{*}_{scat}$ is the conjugate complex number of the scattered electromagnetic field from the object, $\vec{r_i}$ and $\vec{r_j}$ are receiver locations.

The scattered field at any receiver can be computed by applying the Stratton & Chu formulation [21]:

$$\vec{E}_{scat} = \frac{k_0^2}{4\pi}\int_V (\varepsilon(\vec{s}) - \varepsilon_0)\{a\overrightarrow{E_T}(\vec{s}) + \left(b\overrightarrow{E_T}(\vec{s})\cdot\hat{\underline{R}}\right)\hat{\underline{R}}\}\frac{e^{-jk_0R}}{R}dV \tag{2}$$

Where k_0 denotes free-space prorogation constant, $\varepsilon(\vec{s})$ is the complex relative permittivity distribution of target object, ε_0 is the complex relative permittivity of free-space, $a = 1 - j/k_0R - 1/(k_0R)^2$, and $b = -1 + 3j/k_0R + 3/(k_0R)^2$. The total electric field at a point within the target object with position vector $\vec{s}$ can be computed by $\overrightarrow{E_T}(\vec{s}) = \vec{E}_{inc}(\vec{s}) + \vec{E}_{scat}(\vec{s})$.

For N receivers, the total number of complex visibility data is:

$$\vec{V} = \sum_i^N \overrightarrow{V_{i,j}},\ N \geq 3, i \neq j \tag{3}$$

The intensity distribution of an object $I(\vec{s})$ at position $\vec{s}$ is defined [22]:

$$I(\vec{s}) = \left(\frac{k_0^2}{4\pi}\right)^2 |\varepsilon(\vec{s}) - \varepsilon_0|^2 \overrightarrow{E_T}(\vec{s}) \cdot \overrightarrow{E_T^*}(\vec{s}') \tag{4}$$

Referring to Figure 2, a 2D image can be reconstructed by applying the Fourier inversion theorem, which is a projection of the 3D intensity function onto a flat plane in (l, m) space [23].

$$\tilde{I}(l,m) = \iint V(u,v)e^{j2\pi(ul+vm)}\,dldm \tag{5}$$

Where $l = \sin\theta\cos\phi$, $m = \sin\theta\sin\phi$, $u = (\overrightarrow{x_j}) - (\overrightarrow{x_i})/\lambda_0$ and $v = (\overrightarrow{y_j}) - (\overrightarrow{y_i})/\lambda_0$, λ_0 indicates the wavelength in free-space.

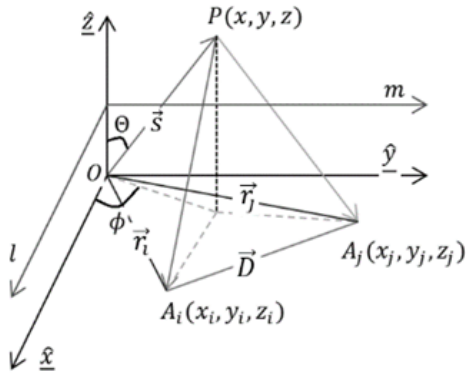

Figure 2. HMI measurement by a pair of receivers.

2.2 Biological tissue-like phantom construction and measurement

2.2.1. Sample preparation

Two types of emulsifying ointment (EO) were prepared. EO-I made of 30% emulsifying wax, 50% white soft paraffin and 20% liquid paraffin. EO-II made of 27% emulsifying wax, 45% white soft paraffin and 18% liquid paraffin and 10% water. Materials were well mixed and shaped in a silicon ice block mould with 12 blocks and each block approximately $10\times10\times10$mm3 dimensions. EO samples were stored in a microwave food container with lid closed after DPs measurement.

Cucumber samples were peeled the skin and cut in cube-shape approximately $15\times15\times10$mm3 dimensions

and weighted averaged 5 gram using a digital kitchen scale. Small blueberries and grapes (4-15mm in diameter) were measured using digital calliper and then selected as samples, all blueberries and grapes samples contained skin. Fresh fruit samples were stored immediately in a microwave food container that fulfilled of EO-I after DPs measurement. All samples were stored at room temperature before and after tests.

2.2.2 DPs measurement procedures and data analysis

DPs of material samples were measured by using an Agilent N5230A VNA with an Agilent 85070D dielectric probe kit. The VNA calibration was done with an open, short, and matched load before the calibration of the probe with measurements on air, a short-circuit block, and glass-distilled water at room temperature of 21°C. During DPs measurement, the probe was pressed against the samples to remove air in the space between samples and probe.

DPs of samples were measured across the 10-20GHz band at room temperature of 21ºC. After each measurement, fruit samples were stored in a microwave food container that fulfilled of EO-I at room temperature for seven days. EO-I and EO-II samples were stored in a microwave food container with lid closed at room temperature for seven days. Seven days later, fruit samples were removed from the container and cleaned by using deionized water. DPs of samples then measured again.

2.2.3 Biological tissue-like phantom construction

The construction of the biological tissue-like phantoms involved three main steps: measurements of selected materials dielectric properties, construction of the individual tissue phantoms using the measured data, finally, merging of the different tissue types into a single complete multilayer tissue model.

Two types of simplified phantoms were developed after analyzing the measured dielectric properties of dielectric materials. A plastic box ($100\times100\times30mm^3$) was used to shape healthy tissue-like phantom (made of EO-II) and a plastic film was used to cover the box. The plastic film has a negligible effect on the scattered field in the measured RF range. Small grapes (4-15mm in diameter) and blueberries (4-7mm in diameter) were inserted into the phantom to simulate malignant tissues. A glass ceramic (MGC) plate (100×100×3mm3) with dielectric constant of 5.67 was used to represent the skin layer.

2.2.4 Imaging measurement of phantoms

The developed phantoms were measured by using the HMI system as presented in section II to generate microwave images. The distance between phantom and the sensor array was 450mm. Background information was measured before measuring the phantom. The magnitude and phase information was measured across the 10-20GHz band. A computer with MATLAB GUI tool was then used to generate and display 2D images of phantom at frequency of 12GHz from the measured data, the imaging algorithm is detailed above.

3. Results

3.1 Dielectric properties of samples

Figure 3 shows the DPs of fresh fruit samples (blueberry, cucumber and grape), EO-I and EO-II across the 10-20GHz band at room temperature of 21oC. Results indicated that DPs of grape, blueberry and two types of EO generally did not vary too much with frequency especially across the 10-15GHz band, dielectric constant of cucumber dropped with increasing frequency while the loss factor of cucumber showed an increasing trend.

Figure 4 and Figure 5 show the DPs of fresh and 7-day old fruits and EO samples, respectively. Results indicated that DPs of all fruit samples slightly dropped with increasing storage time while that of EO samples did not vary with storage time. It is seems that EO can help fruit samples stay fresh and last longer life. The measured values are similar to the contrast between real breast cancer and healthy tissues.

The contract between fruits and EO-II samples is close to that of cancer tissue and healthy tissue, therefore EO-II is more suitable to develop a realistic tissue-like phantom. Compared to grape and blueberry, the dielectric constant of cucumber changed significantly while the contrast between cucumber and EO was greater than 10, thus cucumber was not used to develop a tissue-like phantom.

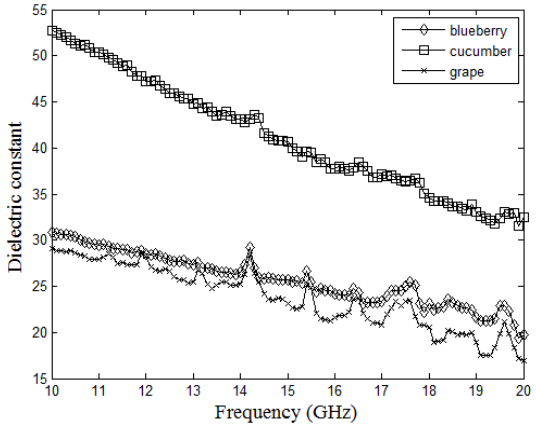

(a)

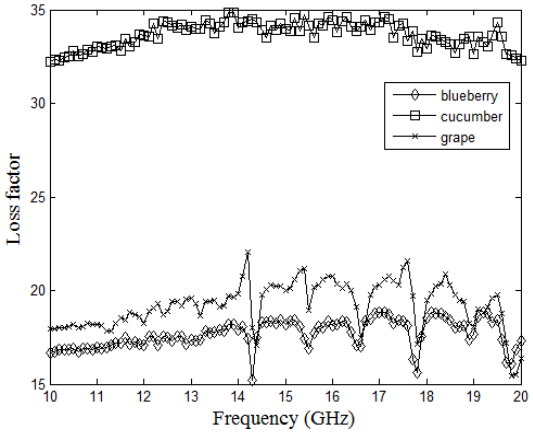

(b)

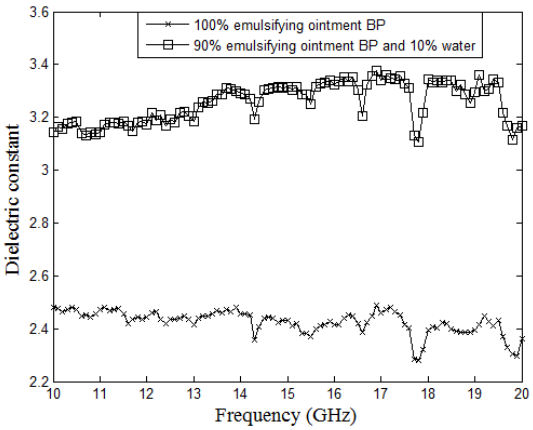

(c)

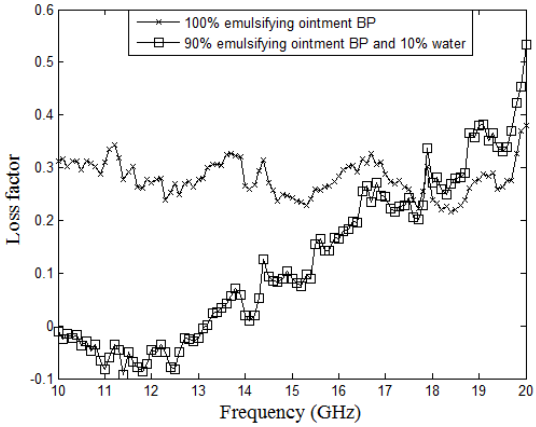

(d)

Figure 3. (a) Dielectric constant of fresh fruits; (b) Loss factor of fresh fruits; (c) Dielectric constant of emulsifying ointment; (d) Loss factor of emulsifying ointment.

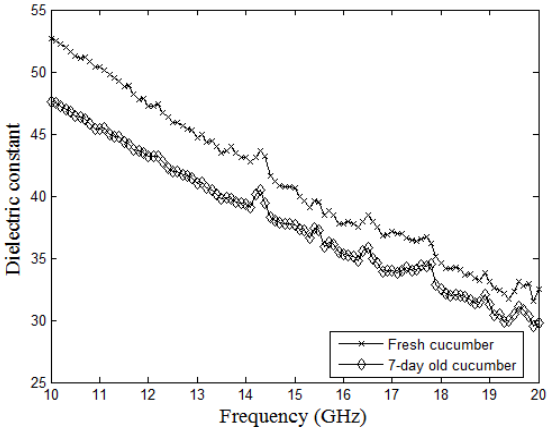

(a)

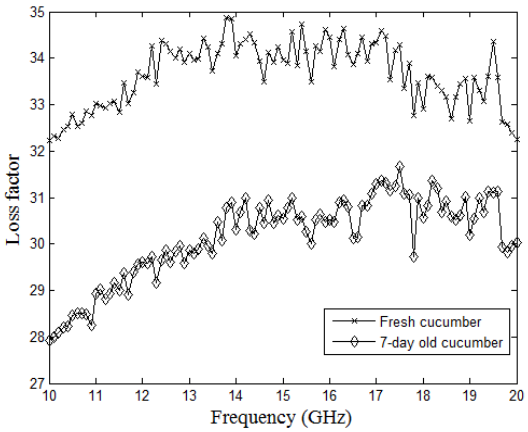

(b)

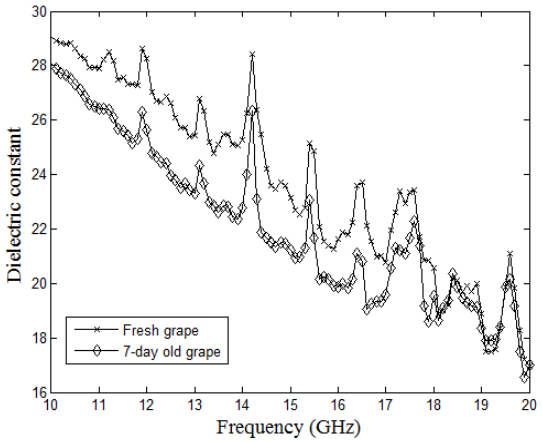

(c)

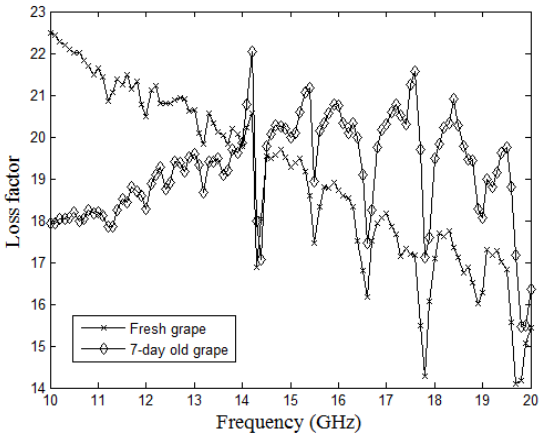

(d)

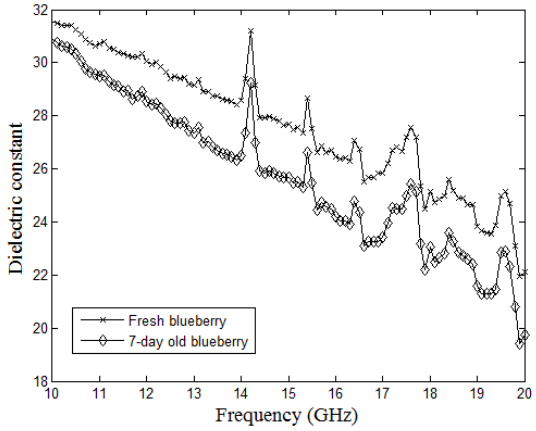

(e)

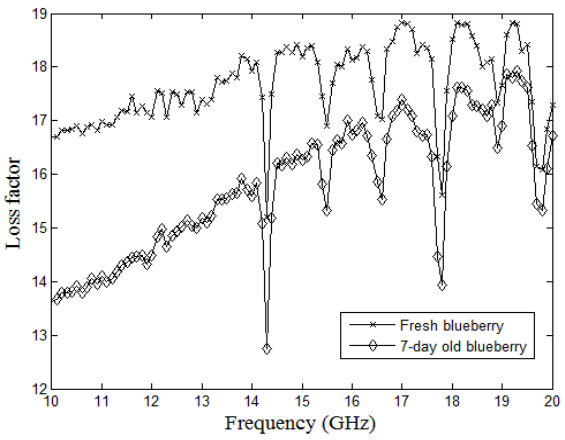

(f)

Figure 4. (a) Dielectric constant of fresh and 7-day old cucumber; (b) Loss factor of fresh and 7-day old cucumber; (c) Dielectric constant of fresh and 7-day old grape; (d) Loss factor of fresh and 7-day old grape; (e) Dielectric constant of fresh and 7-day old blueberry; (f) Loss factor of fresh and 7-day old blueberry.

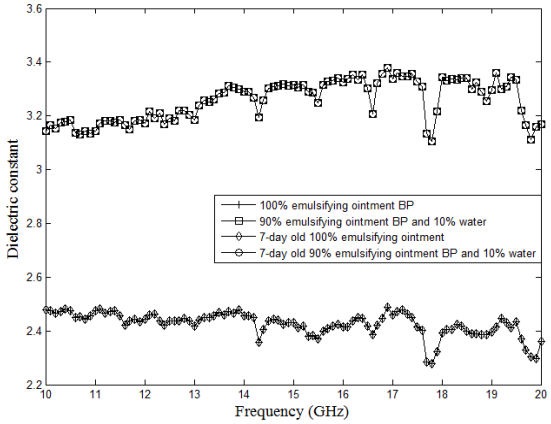

(a)

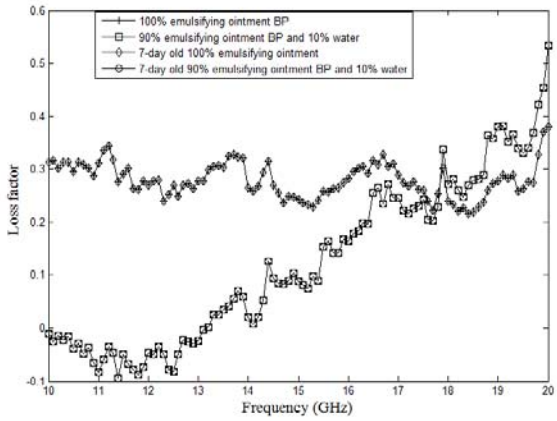

(b)

Figure 5. (a) Dielectric constant of fresh and 7-day old emulsifying ointment; (b) Loss factor of fresh and 7-day old emulsifying ointment.

3.2 Microwave imaging of phantoms

Figure 6 shows the breast phantom contains skin and two lesions that made of grapes, and the reconstructed image that obtained by using HMI measurement system. Lesions were located at (x=50 mm, y=50 mm, z=20 mm) and (x=70 mm, y=80 mm, z=20 mm).

Figure 7 shows the breast phantom of three lesions (made of blueberries) and the reconstructed image that obtained by using HMI measurement system. Color bars plot signal intensity on a linear scale.

(a)

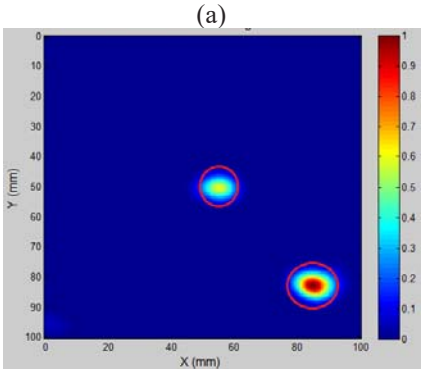

(b)

Figure 6. (a) Breast phantom of two lesions; (b) Reconstructed image.

(a)

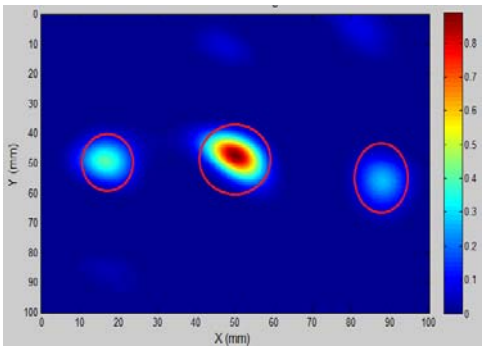

(b)

Figure 7. (a) Breast phantom of three lesions; (b) Reconstructed 2D breast phantom image.

4. Discussion

Two types of simplified biological tissue-like phantoms that contain skin (glass ceramic), healthy tissue (EO-II) and lesions (blueberry, grape) were developed and tested on a HMI system. The measurement results demonstrated that the tissue-like phantom has capability to emulate the characteristics of real breasts. For parametric studies, the contrast between healthy and cancer tissues can be controlled by changing the concentration of water in the healthy mixture phantom. The developed tissue-like phantom is suitable for validation MI techniques with particular focus on breast lesion detection. Potential advantages include non-toxic, low cost, easy to shape, ease of fabrication and have minimum changes in DPs over measurement time.

The practical challenges with the phantom preparation procedure are: 1) difficulty in locating the lesion within the biological tissue-like model; 2) the dielectric contrast of actual healthy tissue and malignant tissue is varying with frequency. The plane location (x-y directions) of a lesion within a biological tissue-like phantom was measured by a ruler, but no depth information (z-direction) was measured. However, it is necessary to produce a 3D image to demonstrate a more realistic result and to validate the MI approaches. Therefore, finding an easy way to identify the location of lesion within a 3D biological tissue-like model and develop a biological tissue-like phantom that is suitable for broadband MI approaches are planned to conduct in the future.

5. Conclusions

This paper presented a method for constructing a tissue-like phantom with DPs similar to those recently reported for breast tissue. The procedure makes significant advances in physiological representation compared to the simplified existing models, allowing for the inclusion of

multiple lesions of varying size embedded within a dielectric object phantom. Experimental results showed that it is possible to generate 2D microwave images of phantom using single frequency of 12GHz. The phantom has a good agreement with the real breast on the contrast between lesion, healthy tissue and skin and has a good stability for at least 7 days at room temperature. Potential advantages include non-toxic, low cost, easy to shape, ease of fabrication and have minimum changes in DPs over measurement time. The research findings have potential to develop a cost-effective tissue-like phantom to investigate the MI approaches.

Acknowledgments

The author gratefully acknowledges the equipment and technical supports from the Institute of Biomedical Technologies (IBTec) at the Auckland University of Technology (AUT), and Callaghan Innovation, Auckland, New Zealand. This work was supported by Natural Science Foundation of Anhui Provence (I708085QH194).

References

[1] P. M. Meaney, M. W. Fanning, D. Li, S. P. Poplack, K. D. Paulsen. "A clinical prototype for active microwave imaging of the breast." IEEE Trans. Microw Theory Tech, 2000, vol.48, no.11, pp.1841–1853.

[2] E. C. Fear, X. Li, S. C. Hagness, M. A. Stuchly. "Conformal microwave imaging for breast cancer detection: Localization of tumors in three dimensions." IEEE Trans. Biomed. Eng, 2002, vol.49, no.8, pp.812–822.

[3] D. Li, P. M. Meaney, K.D. Paulsen. "Conformal microwave imaging for breast cancer detection." IEEE Trans. Microw. Theory Tech, 2003, vol.51, no. 4, pp.1179–1186.

[4] M. Klemm, I.J. Craddock, J.A. Leendertz, A. Preece, R. Benjamin. "Radar-based breast cancer detection using a hemispherical antenna array: Experimental results." IEEE Trans. Antennas Propag, 2009, vol. 57, no. 6, pp.1692–1704.

[5] T. Henriksson, N. Joachimowicz, C. Conessa, J.C. Bolomey. "Quantitative microwave imaging for breast cancer detection using a planar 2.45 GHz system." IEEE Trans. Instrum. Meas., 2010, vol. 59, no. 10, pp.2691–2699.

[6] W.T. Joines, R.L. Jirtle, M.D. Rafal, D.J. Schaefer. "Microwave power absorption differences between normal and malignant tissue." Int. J. Rad. Oncol. Biol. Phys., 1980, vol. 6, pp. 681–687.

[7] S.S. Chaudhary, R.K. Mishra, A. Swarup, J.M. Thomas. "Dielectric properties of normal and malignant human breast tissues at radiowave and microwave frequencies." Indian J. Biochem. Biophys, 1984, vol. 21, pp. 76–79.

[8] A.J. Surowiec, S.S. Stuchly, J.R. Barr, A. Swarup. "Dielectric properties of breast carcinoma and the surrounding tissues." IEEE Transactions on Biomedical Engineering, 1988, vol. 35, no. 4, pp. 257-263.

[9] W.T. Joines, Y. Zhang, C. Li, R.L. Jirtle. "The measured electrical properties of normal and malignant human tissues from 50 to 900 MHz." Medical physics, 1994, vol. 21, no.4, pp.547.

[10] S. Gabriel, R.W. Lau, C. Gabriel. "The dielectric properties of biological tissues: II measurements in the frequency range 10 Hz to 20 GHz." Physics in medicine and biology, 1999, vol.41, no.11, pp. 2251.

[11] S. Gabriel, R.W. Lau, C. Gabriel. "The dielectric properties of biological tissues: III. Parametric models for the dielectric spectrum of tissues." Physics in medicine and biology, 1999, vol. 41, no. 11, pp.2271.

[12] M. Lazebnik, D. Popovic, L. McCartney, C.B. Watkins, M.J. Lindstrom, J. Harter, S.C. Hagness. "A large-scale study of the ultrawideband microwave dielectric properties of normal, benign and malignant breast tissues obtained from cancer surgeries." Physics in Medicine and Biology, 2007, vol. 52, no. 20, pp.6093-6116.

[13] J.J.W. Lagendijk, P. Nilsson. "Hyperthermia dough: a fat and bone equivalent phantom to test microwave/radiofrequency hyperthermia heating systems." Physics in Medicine and Biology, 1985, vol.30, pp.709–712.

[14] C. Marchal, M. Nadi, A.J. Tosser, C.C. Roussey, M.L. Gaulard. "Dielectric properties of gelatin phantoms used for simulations of biological tissues between 10 and 50 MHz." International Journal Hyperthermia, 1989, vol.5, pp.725–732.

[15] M.J. Robinson, M.J. Richardson, J.L. Green, A.W. Preece. "New materials for dielectric simulation of tissues." Phys. Med. Biol, 1991, vol.36, pp.1565–1571.

[16] A. Surowiec, P.N. Shrivastava, M. Astrahan, Z. Petrovich. "Utilization of a multilayer polyacrylamide phantom for evaluation of hyperthermia applicators." Int. J. Hyperthermia, 1992, vol.8, pp.795–807.

[17] Y. Nikawa, M. Chino, K. Kikuchi. "Soft and dry phantom modeling material using silicone rubber with carbon fibre." IEEE Trans. Microw. Theory Tech, 1996, vol.44, pp.1949–1953.

[18] J.T. Chang, M.W. Fanning, P.W. Meaney, K.D. Paulsen. "A conductive plastic for simulating biological tissue at microwave frequencies." IEEE

Trans. Electromagn. Compat., 2000, vol. 42, pp.76–81.

[19] L. Wang, A.M. Al-Jumaily, R. Simpkin. "Investigation of antenna array configurations using far-field holographic microwave imaging technique." Progress in Electromagnetics Research M, 2015, vol. 42, pp. 1-11.

[20] R. Levanda, A. Leshem. "Synthetic aperture radio telescopes." IEEE Signal Processing Magazine, 2010, vol. 27, no. 1, pp. 14-29.

[21] L. Wang, A.M. Al-Jumaily, R. Simpkin. "Imaging of 3-D dielectric objects using far-field holographic microwave imaging technique." Progress in Electromagnetics Research B, 2014, vol. 61, pp.135-147.

[22] S. Silver. Microwave Antenna Theory and Design. S. Peter Peregrinus Ltd, London, UK, 1984, pp.87-90.

[23] M. Born, E. Wolf. Principles of optics: electromagnetic theory of propagation, interference and diffraction of light. CUP Archive, 1999.